Journal of Electronic Materials
https://doi.org/10.1007/s11664-021-09215-w

ORIGINAL RESEARCH ARTICLE

Enhanced Photocatalytic Activity in Strain Engineered Janus WSSe Monolayers

Hemant Verma[1] · Abhijeet J. kale[1] · Chandra Prakash[1] · Moussab Harb[2] · Ambesh Dixit[1]

Received: 14 May 2021 / Accepted: 3 September 2021

Abstract

The relevant fundamental properties of Janus WSSe monolayers to photocatalytic water-splitting performance are presented here and investigated using density functional theory. The Janus WSSe monolayer with a direct band gap of 1.75 eV is subjected to biaxial strain, and related optoelectronic properties are investigated. The effect of strain is reflected in band gap change from direct to indirect. Hydrogen evolution reaction (HER) is active all over, whereas oxygen evolution reaction (OER) is active only at 4% and 6% compressive strains. The red- and blue-shifts under tensile and compressive strains, respectively, substantiate possible control over exciton-phonon interaction making it suitable for the water-splitting application.

Graphic Abstract

Upon being irradiated by sunlight with sufficient energy, the biaxially strained Janus WSSe monolayer complying with HER/OER requirement produces hydrogen gas along with oxygen as a secondary product.

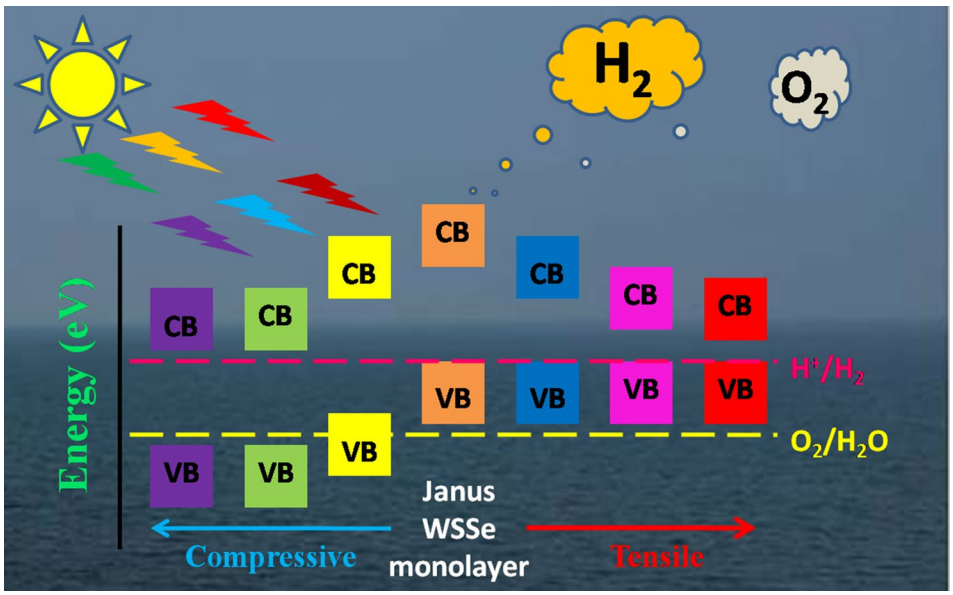

Keywords Janus TMDs monolayer · WSSe · photocatalysis · biaxial strain · HER · OER

Introduction

The energy crisis is currently the most common problem experienced worldwide, and the increasing population is enhancing the severity of this challenge to meet the

✉ Ambesh Dixit
ambesh@iitj.ac.in

Extended author information available on the last page of the article

Published online: 29 September 2021

continuously growing requirements.[1] The high consumption of fossil fuels is a serious concern for the energy sector since fossil fuels are not earth-abundant and are responsible for causing environmental problems such as acid rain, ozone layer destruction, and greenhouse gas emissions.[2] Therefore, eco-friendly and cost-effective energy sources should be explored to replace conventional ones.[3] Hydrogen is considered a clean and renewable energy source. A water-splitting mechanism can generate hydrogen without causing any pollution as the technology generates only oxygen in the gaseous form together with hydrogen.[4] Interestingly, hydrogen has the highest energy density (142 MJ/kg) per unit mass and, thus, a huge potential for clean energy.[5] Water splitting is an emerging technology for hydrogen production that can rival conventional energy producers in the next few decades.[6] Solar energy is an abundant source of energy and is available without any cost. Photo-driven water splitting is, therefore, an efficient, cost-effective method that can be used for the production of hydrogen.[3,7,8] The challenge in this particular technology is to find suitable photocatalysts that are earth-abundant, cost-effective, and efficient. Noble metals are recently reported as an efficient and stable catalyst for water-splitting technology. Yet, these are not suitable for industrial use because of their high cost and low earth abundance.[9] $TiO_2$is one of the first reported photocatalysts operating in the UV spectral region because of its large band gap (~ 3.2 eV).[10] Nowadays, efforts are focused on finding semiconducting photocatalytic materials, which can work in the visible region of the solar spectrum.[11–14]

Two-dimensional transition metal dichalcogenides (2D-TMD) is a promising class of direct band gap semiconducting materials, with a potential impact in photovoltaic devices, light-emitting diodes, lasers, and gas-sensing devices.[15–17] The semiconducting behavior and high adsorption-like features of these materials make them suitable for exploring their photocatalytic performance.[18,19] High surface-to-volume ratio, ultrathin thickness, tunable band gap, and availability of dangling bonds in 2D-TMDs underline their excellent capability in performing overall water splitting.[20]Hydrogen evolution reaction (HER) and oxygen evolution reaction (OER) are the basic reaction mechanisms to understand the photocatalytic water splitting. These are electrochemical process used to generate hydrogen and oxygen from water. Hydrogen can be extracted from water by a cathodic HER, while the anodic OER causes oxidation and thus splitting water, releasing oxygen as:[21]

$$2H^+ + 2e^- \rightarrow H_2 \quad (1)$$

$$2H_2O + 4h^+ \rightarrow O_2 + 4H^+. \quad (2)$$

In photocatalytic water splitting, when photons with energy equal to or larger than the band gap are falling on the material, the number of electrons increases in the conduction band. These electrons are available for migration in the lattice, which causes the generation of partial charge density on the surface of the photocatalytic material. It is essential for the adsorption and desorption of H_2O molecules on the surface of a photocatalyst. The Janus TMD monolayer exhibits its out-of-plane asymmetry, thereby generating an intrinsic dipole moment. It results in charge separation due to opposite partial charges on both sides of the Janus TMD monolayer. Thus, the electric field is set up to enable the photogenerated electrons, upon light irradiation, to drift towards Se atoms and holes toward S atoms.[20] Similarly, the water molecule also exhibits a dipole moment due to the significant difference in electronegativity between oxygen and hydrogen atoms. The oxygen atom in the water molecule carries a partial negative charge while the remaining two hydrogen atoms develop a partial positive charge. These atoms with certain partial charges get attracted toward corresponding opposite partially charged atoms of Janus TMD monolayer. In this way, adsorption of the water molecule occurs on the surface of the Janus TMD monolayer. Thus, the material's photocatalytic efficiency depends on the characteristics such as high absorbance of sunlight, low recombination rate of electron-hole pairs, and adsorption and desorption of OH. The most suitable band gap for higher photocatalytic is ~ 1.23 eV, lying in the visible spectrum. For HER and OER to occur, conduction band minima and valence band maxima should be located higher than H^+/H_2O potential and lower than O_2/H_2O potential, respectively.[22] For enhanced photocatalytic efficiency, several strategies such as bilayer production, strain-engineering, heterostructure construction, and vacancy defect have been reported.[23,24]

A new subclass of 2D-TMDs has emerged, namely 'Janus 2D-TMDs', with their unique properties such as excellent catalytic properties, which enhance hydrogen generation.[25] Recently, the Janus MoSSe monolayer has been theoretically reported as a good candidate for HER at 4% and 6% tensile strain.[26] Selenization or sulfurization can be used to fabricate these Janus materials experimentally for their pristine 2D-TMDs monolayers. Janus 2D-TMDs have an intrinsic dipole because of the out-of-plane asymmetry. Contrarily, conventional TMDs do not possess a dipole moment owing to symmetry. Thus, they cannot effectively separate charges which makes the material inefficient for hydrogen production.[20] This intrinsic dipole separates the conduction and valence band extremum on the different sides of Janus 2D-TMDs, while in the conventional TMDs, valance and conduction band extremum are located in the same area, which favors recombination.[20,26]

The lattice parameters (a, b, and/or c) of the materials directly impact its physical/chemical characteristics when interacting with external stimuli such as photons and an oscillating EM field. Thus, electronic and optical properties

become prone to any changes in structural parameters, and therefore, variation in optical and electronic properties can be attributed to the change in structural properties. Considering this, we aimed to study the impact of tensile and compressive biaxial strains on the material's properties. The results corroborate that electronic properties such as band gap, nature, optical properties, and band edge alignment change with structural parameters. Interestingly, we noticed a direct to indirect band gap transition together with blue- and redshifts in optical transitions. In this article, we report the structural, electronic, and optical properties of the Janus WSSe monolayer together with the impact of both tensile and compressive strains on its photocatalytic performance using density functional theory (DFT). We computed the band gap, band edge alignments, density of states, and imaginary part of the dielectric function to describe the Janus WSSe monolayer's photocatalytic properties. The results reveal that the optoelectronic properties of the Janus WSSe monolayer, when subjected to 4% and 6% biaxial compressive strains, comply with HER and OER requirements, thereby making strain-engineered WSSe a suitable photocatalytic water-splitting system.

Computational Approach

The structural properties of the Janus WSSe monolayer are computed using DFT,[28] with a plane-wave basis approach as implemented in Quantum ESPRESSO.[29] The Perdew-Burke-Ernzerhof (PBE) in generalized gradient approximation (GGA)[30] exchange-correlation functional is used to describe the exchange-correlation functional. The projector augmented wave (PAW) and norm-conserving pseudopotentials are used to calculate the electronic properties. The norm-conserving pseudopotentials[31] are used for computing optical properties, as implemented in Quantum ESPRESSO. The kinetic energy cutoff used for expansion of plane waves is ~50 Ry. Gaussian smearing is used with the broadening of 0.01 Ry. A 12x12x1 k-point Monkhorst-Pack grid is used to represent the Brillouin zone in our calculations. Further, a 2x2x1 supercell is used for Bader charge density calculation. A large vacuum of 25 Å along the Z-axis is introduced to avoid the fictitious interaction of neighboring layers. We fixed the Fermi level at hydrogen reduction potential to understand the band edge alignment, which is -4.44 eV. The CBM and VBM of the strained/unstrained Janus WSSe monolayer are then inspected to check if they meet HER/OER requirements and are then considered suitable or unsuitable for photocatalysis.

Results and Discussion

Structural Analysis

Catalytic properties of a material are strongly dependent on the material's structural stability and the resulting interaction between absorbent and absorbate. Two-dimensional transition metal dichalcogenides are generally available in three polymorphs as 1-T, 2-H, and 3-R.[17,32] In 2D-TMDs, 2-H polymorphs show the most stable characteristics as reported in previous studies.[33] We optimized the Janus WSSe monolayer's structural information, where W is sandwiched between Se and S. We also computed its structural, electronic, and optical properties. The Janus WSSe monolayer has a stable hexagonal structure with trigonal prismatic symmetry. After the complete relaxation, the computed lattice constant and bond length of W-S(W-Se) are 3.23 Å and 2.42 Å (2.53 Å), respectively, and the bond angle between S-W-Se is 82.13°. The consistency of these results with previous reports confirms the reliability of the adopted approach.[34] The optimized structure of the Janus WSSe monolayer is illustrated in Fig. 1 (using XCrySDen)[35,36], which represents a hexagonal structure (2-H), giving the appearance of trigonal prismatic symmetry.

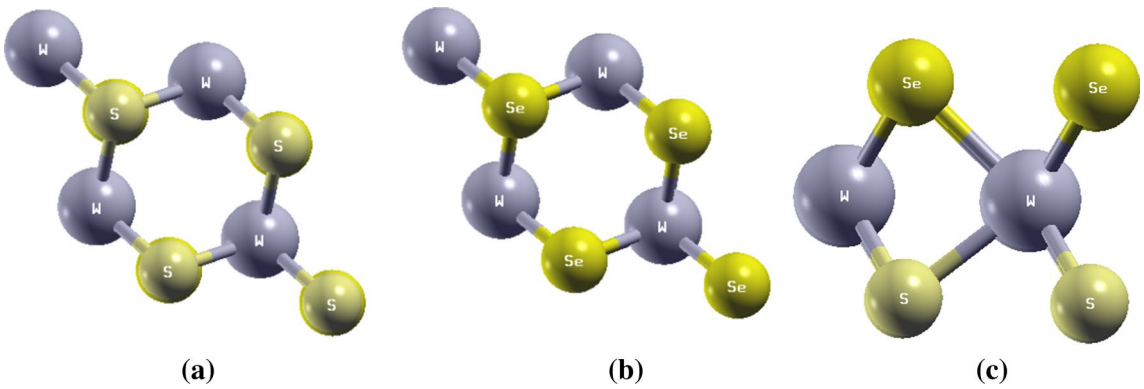

Fig. 1 Top, bottom, and side view of the Janus WSSe monolayer (from left to right).

Electronic Properties

For photocatalysis, photogenerated charge carrier availability is essential, and the difference between conduction band (CB) minima and valence band (VB) maxima plays a vital role in this regard which can be understood more clearly by the electronic band structure of the materials. For this reason, we examined the band structure of the Janus WSSe monolayer and observed the effect of strain on the electronic properties.[26]

The unstrained band structure is plotted along Γ–K–M–Γ; Fig. 2a. The band gap for the unstrained system computed using GGA-PBE with PAW pseudopotentials is ~ 1.75 eV. Moreover, we also performed this calculation using norm-conserving pseudopotentials and no significant difference is observed in the band gap (~ 1.76 eV). These results are consistent with the previous results.[9,33,37] Generally, PBE underestimates the band gap values. However, the PBE result (1.59 eV) for the Janus MoSSe monolayer is in good agreement with its experimental band gap (1.68 eV).[26,27] Moreover, it should be noted that the HSE06 result (2.09 eV) for the Janus MoSSe monolayer is much larger than the reported experimental band gap value. The

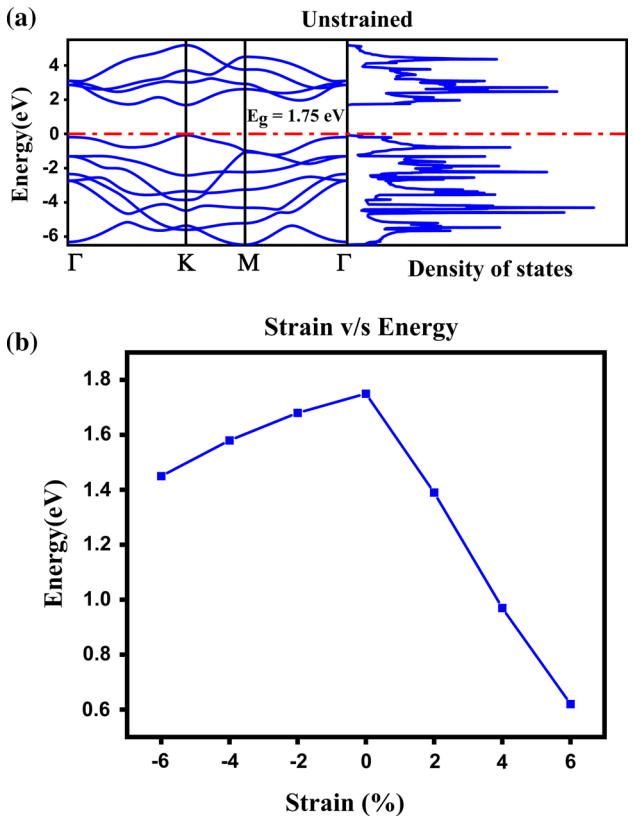

Fig. 2 (a) Band structure of the Janus WSSe monolayer with the total density of states (b) Variation in band gap with tensile and compressive strain.

Janus WSSe monolayer is similar to the Janus MoSSe monolayer except that Mo is replaced by W. The accuracy (in view of the aforementioned 2D-TMDs) and requirement of relatively less computational power, we relied on PBE XC functional-based calculations in our work.

The Janus WSSe monolayer is stable when unstrained and over a range of compressive and tensile strains.[37,38] Therefore, after studying the unstrained system, we applied a range of biaxial strains on the Janus WSSe monolayer to investigate its impact on band gap and other electronic properties. The variation in the band gap with the strain is also summarized in Fig. 2b. The band structures at 2%, 4%, and 6% tensile and compressive strains are plotted along the same high symmetry path, Fig. 3. The strained Janus WSSe monolayer shows a direct to indirect band gap transition under strains and rapidly lowers the band gap values under tensile strains. On the other hand, band gap values slowly decrease under compressive strains. In addition, earlier research reports suggest the band gap tunability and electronic transitions by applying strain in WSSe.[39,40] For the overall water-splitting reaction, the semiconductor material should have a band gap value larger than 1.23 eV.[9,23] Our results suggest that the Janus WSSe monolayer has a suitable band gap for both unstrained and strained cases, with wide tunability. The 2% tensile strained Janus WSSe monolayer is more suitable for photocatalytic application.

The ideal photocatalytic material should show both HER and OER for efficient splitting of the water molecule. The CBM should be higher than H^+/H_2 potential and VBM should be lower than and O_2/H_2O potential to realize both HER and OER simultaneously. The computed band edge alignments for both unstrained and strained Janus WSSe monolayers are summarized in Fig. 4, They show that the unstrained system is suitable for HER only. Interestingly, the Janus WSSe monolayer shows HER activity at 2%, 4%, and 6% for both tensile and compressive strain, while OER is active only at 4% and 6% compressive strain. For an ideal photocatalyst, both HER and OER activity should be present simultaneously with a suitable band gap value. Here, 4% and 6% compressive strains of Janus WSSe monolayers show both HER and OER activity with a suitable band gap, making it a relatively more promising photocatalyst for the overall water-splitting application.

We also computed the projected density of states to understand the orbital contribution to the VBM and CBM of the Janus WSSe monolayer band structure. The results are shown in Fig. 5a, suggesting that the tungsten d orbitals mainly dominate the CBM. However, there is a considerable overlap of S and Se p orbitals in the VBM formation. Similar characteristics noted for CBM formation are mainly due to the hybridization of W d-, S p-, and Se p-orbitals, causing a covalent bond between W and S/Se atoms.

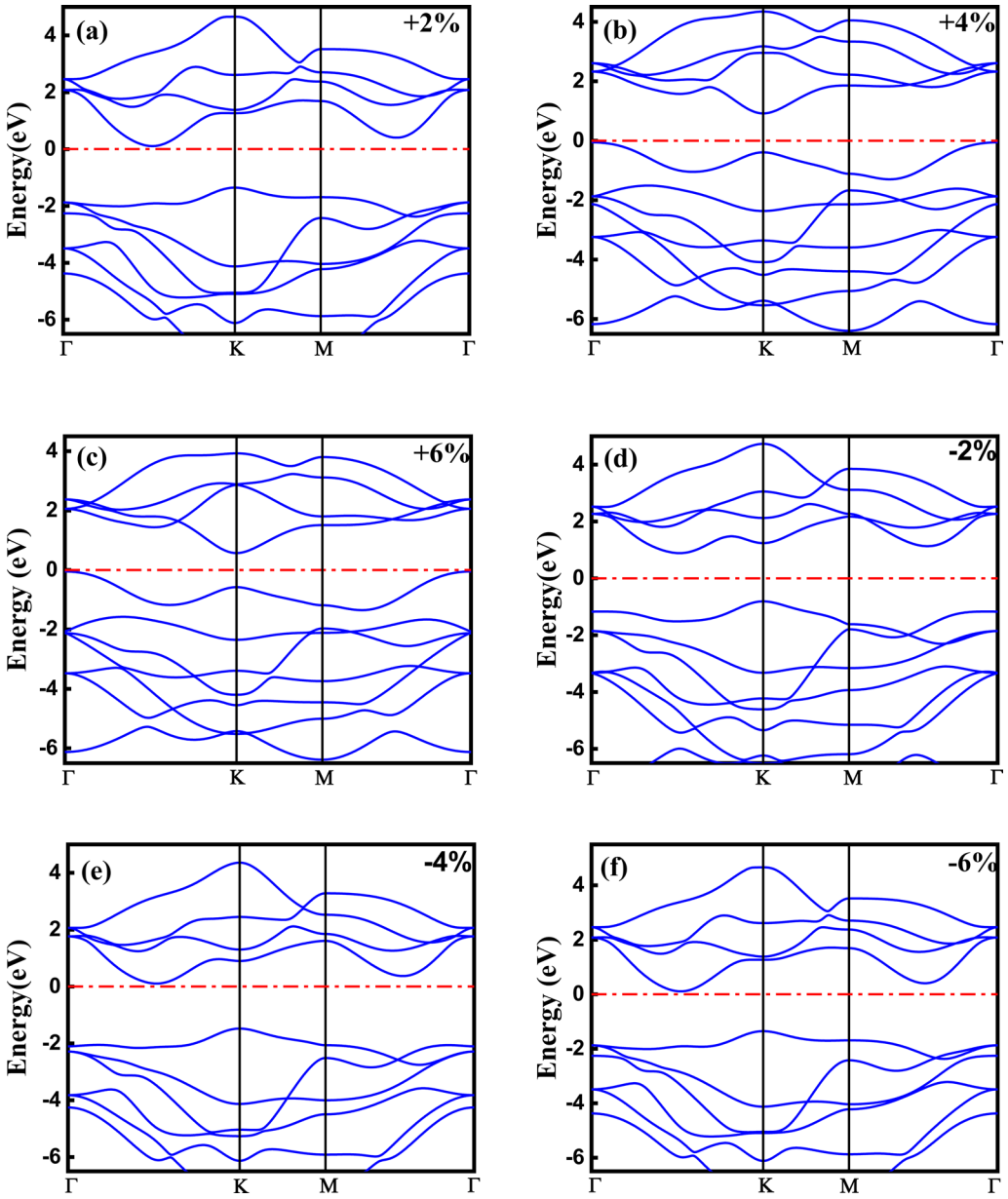

Fig. 3 Band structure of the strained Janus WSSe monolayer at tensile strain (a) 2% (b) 4% (c) 6% and compressive strain (d) 2% (e) 4% (f) 6%.

The optical response of the material, particularly the photon absorption or emission process, is determined by the number of available states for photon-matter interaction. Joint density of states plot gives us this information on the number of available states for the particular energy/frequency and is calculated by,

$$J(\omega) = \sum_{\alpha}\sum_{\beta}\frac{V}{(2\pi)^3}\int \delta\left(E_{k,\beta} - E_{k,\alpha} - \hbar\omega\right) - \left[f\left(E_{k,\alpha}\right) - f\left(E_{k,\beta}\right)\right]\cdot d^3k \tag{3}$$

where α and β are the respective states of conduction and valence band, E_k represents the eigenvalues of the Hamiltonian, V, and $f(.)$ represent cell volume and Fermi distribution function, respectively. The trickier part of this equation, the Dirac delta function, is made tractable by approximating it using the Gaussian distribution function.[41] The DOS plot

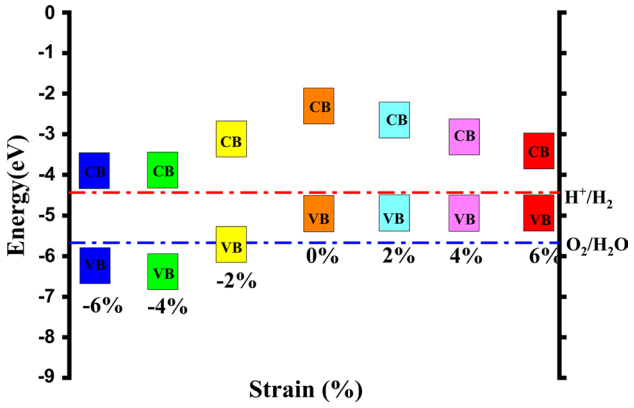

Fig. 4 Band edge alignments of the Janus WSSe monolayer with tensile and compressive strain.

in Fig. 5 corroborates the redshift and blueshift in tensile and compressive strain cases, as discussed later in the optical properties subsection. The DOS plot for the tensile case shows peaks separated by larger energy differences than those in the compressive case, which is consistent with the computed band gap variation under strain (Fig. 2b). Moreover, peaks for compressive cases are relatively sharper and greater in amplitude than peaks of tensile systems. The DOS (Fig. 5) results suggest the maximum optical activity in the far IR-visible and UV regions for tensile and compressive strained Janus WSSe monolayers.

Optical Properties

Photocatalysis uses solar energy to split water molecules into constituent hydrogen and oxygen molecules. Thus, the absorption of solar energy becomes a critical factor, and it is imperative to check the material's optical response to incoming light, i.e., optical properties. The optical properties are computed under the approximations when electrons are assumed to respond merely to the perturbing external potential, together with a single frequency oscillation and the screening potential. This approximation is termed a random phase approximation.[42] This approach with a self-consistent field method generates a dynamic dielectric function that depends on external perturbation frequency and averaged total electric potential at the particular wave vector

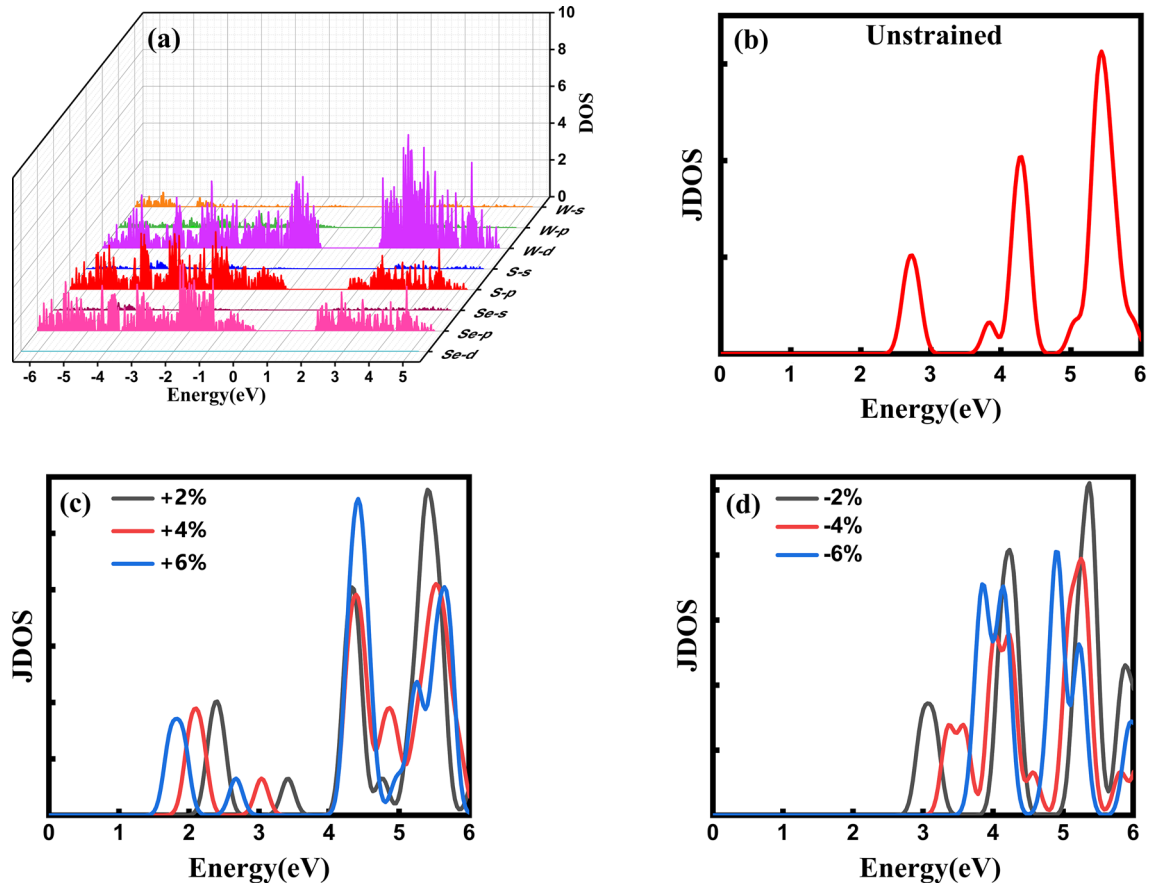

Fig. 5 (a) Projected density of states of the Janus WSSe monolayer and the joint density of states of the Janus WSSe monolayer for (b) unstrained (c) tensile strain (d) compressive strain position.

k. The optical absorption data is complemented or strengthened by the imaginary part of the dielectric function.[43] Figure 6 displays the imaginary part of the dielectric constant against energy for the unstrained and strained Janus WSSe monolayers.

The first high peak is located at 2.79 eV for the unstrained Janus WSSe monolayer system, which shifts towards higher and lower energy depending on the type of strains. This first high peak is located at 2.31, 2.17, and 1.74 eV for 2%, 4%, and 6% tensile strained Janus WSSe monolayers, respectively. Contrarily, the first high peaks for compressive 2%, 4%, and 6% strained Janus WSSe monolayers are obtained at 3.01, 3.36, and 5.22 eV, respectively. Thus, a blueshift and a redshift are ovbserved for compressive and tensile strained Janus WSSe monolayers, respectively. A similar trend has already been reported for the Janus MoSSe monolayer.[26] This similarity in the energy shift is attributed to the similarity in the crystal class for both Janus WSSe and MoSSe monolayers. Figure 6a represents the imaginary part of dielectric function for unstrained Janus WSSe monolayer, whereas Fig. 6b and c shows the imaginary part for the tensile and compressive strained WSSe monolayers. The results clearly indicate red- and blueshifts. The imaginary part of the dielectric constant suggests the maximum possible absorption or optical transitions in far IR and visible region for tensile cases and UV region for compressive strains, in accordance with the DOS results. Apart from the red- and blueshift, there is another distinction between the imaginary part of tensile and compressive strains, which is characterized by the amplitude and energetic distribution of peaks.

The absorption of solar light is also an essential factor in enhancing solar-to-hydrogen (STH) efficiency. The efficiency of sunlight absorption is defined as the output and input ratio of solar energy flux as:

$$\eta_{\text{absorption}} = \frac{\int_{E_g}^{\infty} P(\hbar\omega)d(\hbar\omega)}{\int_{0}^{\infty} P(\hbar\omega)d(\hbar\omega)} \tag{4}$$

where E_g is the band gap value of the semiconductor photocatalyst, and $P(\hbar\omega)$ is the solar energy flux of energy of $\hbar\omega$ at AM1.5 G solar spectrum.[20] Table I presents the band gap values of the Janus WSSe monolayer computed using the above equation at the various strained and unstrained

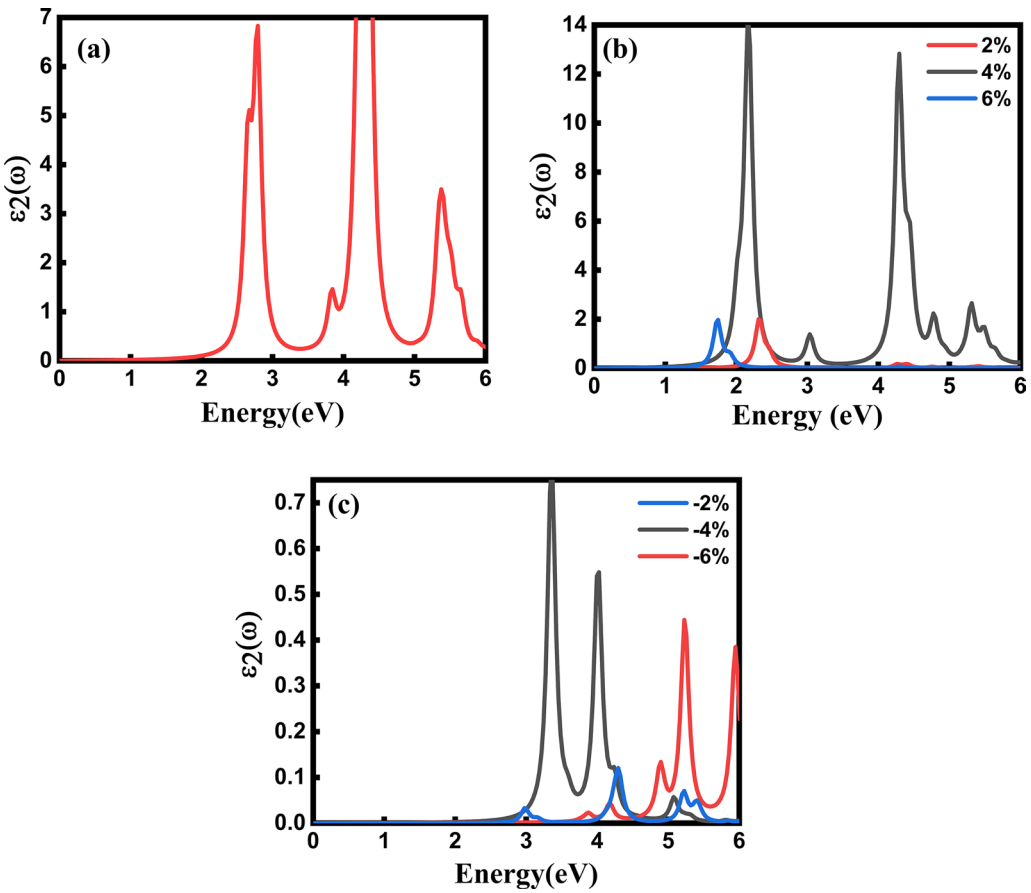

Fig. 6 Imaginary part of the dielectric function of the Janus WSSe monolayer at (a) unstrained position (b) tensile strained system (c) compressive strained system.

Table I Energy band gap and corresponding wavelengths for the Janus WSSe monolayer at different strains and at the unstrained condition and the resultant calculated efficiency of sunlight absorption by the Janus WSSe monolayer

Strain (%)	Band gap (eV)	Wavelength (nm)	Sunlight absorption efficiency (%)
− 6	1.45 (indirect)	855	35
− 4	1.58 (indirect)	785	42
− 2	1.68 (indirect)	738	47
0	1.75 (direct)	708	51
2	1.39 (indirect)	892	32
4	0.97 (indirect)	1278	13
6	0.62 (indirect)	2000	3.7

conditions together with their corresponding wavelengths and sunlight absorption efficiency.

From Table I, it is clear that unstrained Janus WSSe monolayer exhibits maximum $\eta_{absorption}$ around 51%. This absorption efficiency starts decreasing with increasing compressive and tensile strains. The tensile strain exhibits a relatively more adverse effect on $\eta_{absorption}$ as it rapidly drops and reaches around 3.7% for 6% tensile strain. The Janus WSSe monolayer appears to tolerate compressive strain relatively better and maintains absorption efficiency up to 35% for a maximum even at 6% compressive strain. Thus, together, the unstrained and compressively strained Janus WSSe monolayer may show better prospects for enhanced photocatalytic activity.

For water splitting, the adsorption of water molecules on the surface of photocatalytic material is necessary. The efficacy of the Janus WSSe monolayer is influenced by the basal planes.[44] Therefore, we worked out the adsorption energy and charge transfer on the basal plane of the Janus WSSe monolayer. To ensure the adsorption of water molecules, the adsorption energy (E_{ads}) is computed as,[44]

$$E_{ads} = E_{total} - E_{adsorbate} - E_{adsorbent} \quad (5)$$

where E_{total} is the energy of the whole system, $E_{adsorbate}$ is the energy of WSSe, and $E_{adsorbent}$ is the energy of the H_2O molecule. A negative value of E_{ads} indicates good adsorption, whereas positive E_{ads} favors weak adsorption. The computed adsorption energy E_{ads} is − 0.021eV, thus substantiating the good adsorption and desorption on the surface site of the adsorbent.[44] The adsorption picture becomes clearer using Bader charge density distribution. A 2×2×1 supercell of the Janus WSSe monolayer was also considered to model the water molecule's adsorption on the Janus WSSe monolayer and to compute Bader charge density. The computed Bader charge density is thus plotted using VESTA and shown in Fig. 7.[45]

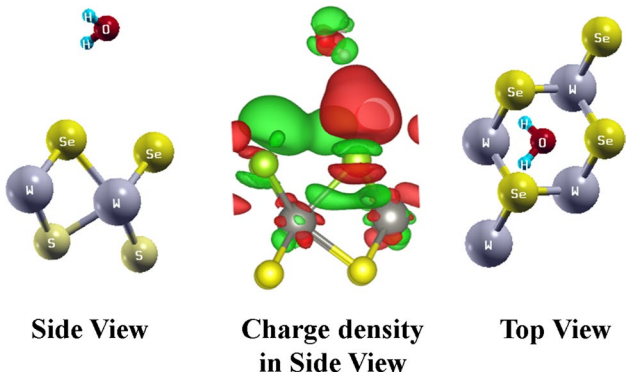

Fig. 7 Adsorption of water molecule on the Janus WSSe monolayer described by charge density distribution (here positive and negative isosurfaces are shown in red and green, respectively) (Color figure online)

The charge transfer mechanism between the adsorbent Janus WSSe monolayer and adsorbate H_2O can be investigated from the electronic charge isosurface analysis using the Bader charge density difference between the adsorbate and the adsorbent. In Fig. 6, red and green indicate the positive and negative isosurfaces for the charge density. The charge density difference (CDD) is calculated as,

$$CDD = \text{charge density}_{(WSSe+H_2O)} - \text{charge density}_{(WSSe)} - \text{charge density}_{(H_2O)} \quad (6)$$

The calculated value of Bader charge density is +0.0001e. The charge transfer may be or may not be possible here due to the smaller Bader charge density. However, the previous adsorption results favor the charge transfer with a small value of Bader charge density.[46,47] This small value indicates the poor charge transfer due to the poor activity of the basal plane in the Janus WSSe monolayer. A positive value for the Bader charge density difference indicates the release of electrons from the adsorbed water molecule. Also, there is an accumulation of charge on the WSSe surface for H_2O, denoting charge-donor properties of water molecules, as shown in Fig. 6.

Conclusion

We investigated the structural and optoelectronic properties of the Janus WSSe monolayer using DFT to understand the impact of strain on its photocatalytic characteristics for water-splitting application. The Janus WSSe monolayer exhibits a suitable band gap for water-splitting application together with probable HER activity. We noticed HER activity for 2%, 4%, and 6% compressive and tensile

strained Janus WSSe monolayers, whereas an OER activity is observed for 4% and 6% compressive strained Janus WSSe monolayers. Further, red- and blueshifts are noted with tensile and compressive strains, respectively. The 4% and 6% compressive strained Janus WSSe monolayer with suitable band gap and relative band edge positions shows the potential for hydrogen generation. Thus, the observed results suggest that strain can be used as an external parameter for modulating the electronic properties in such a way that both HER and OER activities can be realized efficiently in a Janus WSSe monolayer.

Acknowledgments Author Ambesh Dixit acknowledges the funding agency Science & Engineering Research Board (SERB), Department of Science and Technology, Government of India, through project # CRG/2020/004023 for carrying out this work. Hemant Verma acknowledges HPC facilities at IIT Jodhpur and Mr. Ram Milan Sahani, Mr. Sumit Kukreti, Ms. Surbhi Ramawat, Ms. Priyambada Sahoo, Mr. Ram Niwas Kumhar, and Mr. Harsh Jain for their fruitful discussion during the work.

Conflict of interest The authors declare that they have no conflict of interest.

References

1. D.G. Nocera, and M.P. Nash, *Proc. Natl. Acad. Sci. U. S. A.* 103, 15729 (2006).
2. X. Ou, X. Zhang, and S. Chang, *Energy Policy* 38, 406 (2010).
3. Z. Zhao, R.V. Goncalves, S.K. Barman, E.J. Willard, E. Byle, R. Perry, Z. Wu, M.N. Huda, A.J. Moulé, and F.E. Osterloh, *Energy Environ. Sci.* 12, 1385 (2019).
4. A. Kudo, and Y. Miseki, *Chem. Soc. Rev.* 38, 253 (2009).
5. R. Tong, K.W. Ng, X. Wang, S. Wang, X. Wang, and H. Pan, *J. Mater. Chem. A* 8, 23202 (2020).
6. V. Kumaravel, S. Mathew, J. Bartlett, and S.C. Pillai, *Appl. Catal. B* 244, 1021 (2019).
7. Y. Li, Y.K. Peng, L. Hu, J. Zheng, D. Prabhakaran, S. Wu, T.J. Puchtler, M. Li, K.Y. Wong, R.A. Taylor, and S.C.E. Tsang, *Nat. Commun.* 10, 1 (2019).
8. J. Ran, J. Zhang, J. Yu, M. Jaroniec, and S.Z. Qiao, *Chem. Soc. Rev.* 43, 7787 (2014).
9. L. Ju, M. Bie, X. Tang, J. Shang, and L. Kou, *ACS Appl. Mater. Interfaces* 12, 29335 (2020).
10. X. Chen, L. Liu, P.Y. Yu, and S.S. Mao, *Science* 331, 746 (2011).
11. S. Ould-Chikh, O. Proux, P. Afanasiev, L. Khrouz, M.N. Hedhili, D.H. Anjum, M. Harb, C. Geantet, J.M. Basset, and E. Puzenat, *Chemsuschem* 7, 1361 (2014).
12. K. Maeda, and K. Domen, *Theor. Comput. Chem.* 18, 301 (2007).
13. K. Maeda, *J. Photochem. Photobiol. C* 12, 237 (2011).
14. M. Ni, M.K.H. Leung, D.Y.C. Leung, and K. Sumathy, *Renew. Sustain. Energy Rev.* 11, 401 (2007).
15. M. Shanmugam, R. Jacobs-Gedrim, E.S. Song, and B. Yu, *Nanoscale* 6, 12682 (2014).
16. F. Withers, O. Del Pozo-Zamudio, A. Mishchenko, A.P. Rooney, A. Gholinia, K. Watanabe, T. Taniguchi, S.J. Haigh, A.K. Geim, A.I. Tartakovskii, and K.S. Novoselov, *Nat. Mater.* 14, 301 (2015).
17. R. Li, Y. Cheng, and W. Huang, *Small* 14, 1 (2018).
18. Y. Li, S. Wu, J. Zheng, Y.K. Peng, D. Prabhakaran, R.A. Taylor, and S.C.E. Tsang, *Mater. Today* 41, 34 (2020).
19. M.R. Hoffmann, S.T. Martin, W. Choi, and D.W. Bahnemann, *Chem. Rev.* 95, 69 (1995).
20. L. Ju, M. Bie, J. Shang, X. Tang, and L. Kou, *J. Phys. Mater.* 3, 022004 (2020).
21. A. Lasia, in *Handbook Fuel Cells* (Wiley, 2010).
22. A. L. Linsebigler, G. Lu, and J. T. Yates, *Chem. Rev.* 95, 735 (1995).
23. P. Ganguly, M. Harb, Z. Cao, L. Cavallo, A. Breen, S. Dervin, D.D. Dionysiou, and S.C. Pillai, *ACS Energy Lett.* 4, 1687 (2019).
24. Z. Cao, M. Harb, S. Lardhi, and L. Cavallo, *J. Phys. Chem. Lett.* 8, 1664–1669 (2017).
25. X. Ma, X. Wu, H. Wang, and Y. Wang, *J. Mater. Chem. A* 6, 2295 (2018).
26. T.N. Do, C.V. Nguyen, M. Idrees, B. Amin, H.A. Tam, N.N. Hieu, H.V. Phuc, and L.T. Hoa, *Optik* 224, 165503 (2020).
27. F. Chen, H. Huang, L. Guo, Y. Zhang, and T. Ma, *Angew. Chem. Int. Ed.* 58, 10061 (2019).
28. L.J. Sham, and M. Schlter, *Phys. Rev. Lett.* 51, 1888 (1983).
29. P. Giannozzi, S. Baroni, N. Bonini, M. Calandra, R. Car, C. Cavazzoni, D. Ceresoli, G.L. Chiarotti, M. Cococcioni, I. Dabo, A. Dal Corso, S. De Gironcoli, S. Fabris, G. Fratesi, R. Gebauer, U. Gerstmann, C. Gougoussis, A. Kokalj, M. Lazzeri, L. Martin-Samos, N. Marzari, F. Mauri, R. Mazzarello, S. Paolini, A. Pasquarello, L. Paulatto, C. Sbraccia, S. Scandolo, G. Sclauzero, A.P. Seitsonen, A. Smogunov, P. Umari, and R.M. Wentzcovitch, *J. Phys. Condens. Matter* 21, 395502 (2009).
30. J.P. Perdew, K. Burke, and M. Ernzerhof, *Phys. Rev. Lett.* 78, 1396 (1997).
31. D.R. Hamann, M. Schlüter, and C. Chiang, *Phys. Rev. Lett.* 43, 1494 (1979).
32. M. Chhowalla, H.S. Shin, G. Eda, L.J. Li, K.P. Loh, and H. Zhang, *Nat. Chem.* 5, 263 (2013).
33. R. Chaurasiya, G.K. Gupta, and A. Dixit, *Solar Energy Mater. Solar Cells* 201, 110076 (2019).
34. J. Guo, C. Ke, and Y. Wu, *Nanoscale Res. Lett.* 15, 97 (2020).
35. A. Kokalj, *Comput. Mater. Sci.* 28, 155 (2003).
36. A. Kokalj, *J. Mol. Graph. Model.* 17, 176 (1999).
37. R. Chaurasiya, A. Dixit, and R. Pandey, *Superlattices Microstruct.* 122, 268 (2018).
38. R. Chaurasiya, S. Tyagi, N. Singh, S. Auluck, and A. Dixit, *J. Alloys Compd.* 855, 157304 (2021).
39. A.J. Lu, R.Q. Zhang, and S.T. Lee, *Appl. Phys. Lett.* 91, 263107 (2007).
40. C. Zhang, A. De Sarkar, and R.Q. Zhang, *J. Phys. Chem. C* 115, 23682 (2011).
41. A. Sengupta, *Phys. Scr.* 94, 125806 (2019).
42. A. Benassi, A. Ferretti, C. Cavazzoni, PWSCFs epsilon.x user's manual.
43. J. Petzelt and I. Rychetskỳ, Encyclopedia of Condensed Matter Physics 426 (2005).
44. N.N. Som, and P.K. Jha, *Int. J. Hydrogen Energy* 45, 23920 (2020).
45. K. Momma, and F. Izumi, *J. Appl. Crystallogr.* 41, 653 (2008).
46. R. Hou, Y. Xia, and S. Yang, *ACS Omega* 5, 26748 (2020).
47. F. Azouvi, *Revue Internationale d'histoire de La Psychiatrie* 2, 5 (1984).

Authors and Affiliations

Hemant Verma[1] · Abhijeet J. kale[1] · Chandra Prakash[1] · Moussab Harb[2] · Ambesh Dixit[1]

[1] Department of Physics, Indian Institute of Technology Jodhpur, Jodhpur 342037, India

[2] KAUST Catalysis Center, Physical Sciences and Engineering Division, King Abdullah University of Science and Technology (KAUST), 4700 KAUST, Thuwal 23955-6900, Kingdom of Saudi Arabia